

Ultrasound Sensing Can Improve Continuous Classification of Discrete Ambulation Modes Compared to Surface Electromyography

Kaitlin G. Rabe , Student Member, IEEE, Mohammad Hassan Jahanandish , Jacob R. Boehm, Student Member, IEEE, Ann Majewicz Fey, Member, IEEE, Kenneth Hoyt, Senior Member, IEEE, and Nicholas P. Fey, Member, IEEE

Abstract—Clinical translation of "intelligent" lower-limb assistive technologies relies on robust control interfaces capable of accurately detecting user intent. To date, mechanical sensors and surface electromyography (EMG) have been the primary sensing modalities used to classify ambulation. Ultrasound (US) imaging can be used to detect user-intent by characterizing structural changes of muscle. Our study evaluates wearable US imaging as a new sensing modality for continuous classification of five discrete ambulation modes: level, incline, decline, stair ascent, and stair descent ambulation, and benchmarks performance relative to EMG sensing. Ten able-bodied subjects were equipped with a wearable US scanner and eight unilateral EMG sensors. Time-intensity features were recorded from US images of three thigh muscles. Features from sliding windows of EMG signals were analyzed in two configurations: one including 5 EMG sensors on muscles around the thigh, and another with 3 additional sensors placed on the shank. Linear discriminate analysis was implemented to continuously classify these phase-dependent features of each sensing modality as one of five ambulation modes. US-based sensing statistically improved mean classification accuracy to 99.8% (99.5-100% CI) compared to 8-EMG sensors (85.8%; 84.0-87.6% CI) and 5-EMG sensors (75.3%; 74.5-76.1% CI). Further, separability analyses show the importance of superficial and deep US information for stair classification relative to other modes. These results are the first to demonstrate the ability of US-based sensing to classify discrete ambulation modes, highlighting the potential for improved assistive device

Manuscript received March 5, 2020; revised June 19, 2020 and August 14, 2020; accepted September 29, 2020. Date of publication October 21, 2020; date of current version March 19, 2021. This work was supported by the National Science Foundation under the Award Number 1925343. (Corresponding author: Nicholas Fey.)

Kaitlin G. Rabe is with the Department of Biomedical Engineering, The University of Texas Austin.

Mohammad Hassan Jahanandish is with the Department of Bioengineering, The University of Texas Dallas.

Jacob R. Boehm and Ann Majewicz Fey are with the Department of Mechanical Engineering, The University of Texas Austin.

Kenneth Hoyt is with the Department of Bioengineering, The University of Texas Dallas.

Nicholas P. Fey is with the Department of Mechanical Engineering and the Department of Biomedical Engineering, The University of Texas Austin, Austin, TX 78712 USA, and also with the Department of Physical Medicine and Rehabilitation, UT Southwestern Medical Center, Dallas, TX 75390 USA (e-mail: nicholas.fey@utdallas.edu).

Digital Object Identifier 10.1109/TBME.2020.3032077

control using less widespread, less superficial and higher resolution sensing of skeletal muscle.

Index Terms—Assistive technology, electromyography, ultrasound.

I. INTRODUCTION

N ESTIMATED 12.3 million people over the age of six years needed assistance with activities of daily living in the United States in 2010. Furthermore, 1.9 million people were living with limb loss and annual hospital costs associated with these individuals total more than \$9 billion [1]. Aging, obesity and the development of vascular and other diseases (e.g. osteosarcoma) have led to projections that the number of individuals with limb loss will double by 2050 [2]. Wearable assistive devices aiming to restore "natural" locomotor abilities during a wide sampling of daily tasks are essential for improving the quality of life of individuals with mobility impairments.

To date, the most common assistive devices clinically available to patients with disability affecting the lower-limb are conventional passive devices or devices that are controlled via a microprocessor. Currently, most lower-limb assistive devices rely on mechanical sensors for detection of motion and require the user to manually identify and switch the ambulation mode of the device [3], [4]. This requirement for manual control is burdensome and inconvenient to the user. Mechanically-powered (i.e. robotic) assistive devices are capable of generating and transmitting net mechanical energy to their users in order to restore the ability to perform dynamic locomotor tasks of heightened mechanical demands. A recent literature review evaluated 21 powered lower-limb assistive devices and concluded that the lack of a robust control system that can accurately recognize user intent is a significant limiting factor for potential users [5]. To improve functionality and clinical translation of assistive devices, a robust and intuitive control interface (i.e. capable of continuously detecting ambulation mode and seamlessly transitioning between various modes without direct user input) is required.

Many researchers have investigated the use of surface electromyography (EMG) and machine learning models, or pattern recognition classifiers, for ambulation mode detection and assistive device control. Surface EMG has primarily been suggested as an intuitive sensing interface due to its noninvasive

0018-9294 © 2020 IEEE. Personal use is permitted, but republication/redistribution requires IEEE permission. See https://www.ieee.org/publications/rights/index.html for more information.

ability to measure muscle excitation [6], [7]. These studies have generated promising results indicating the inclusion of EMG from many (≥ 5) muscle sites around the thigh and/or lowerlimb, along with information from mechanical sensors improved classification accuracy of ambulation modes; however, substantial errors remain in misclassifying ambulation mode [8], [9]. These errors may be attributed to EMGs reliance on superficial muscle recordings, the inability to differentiate between relative muscle firing of adjacent muscles resulting in susceptibility to muscle crosstalk [10], as well as susceptibility to motion and environmental conditions of the skin interface [11]. To robustly handle these limitations, classification approaches that interpret EMG and mechanical sensors are usually phase-based, such that decisions are only made at specific events within the gait cycle (e.g. heel strike and toe off), or incorporate sensor fault detection to increase class separability [12], [13]. The performance of lower-limb assistive technologies may improve if such devices are able to interpret transitions between classes continuously. Continuous classification could allow for users to react to perturbations during gait and seamlessly transition between ambulation modes. However, continuous classification is more difficult during ambulation due to the non-stationary nature of both neural and mechanical signals during each stride. Thus, there may be other sensing modalities that offer equivalent or improved performance with less widespread sensing requirements while also enabling continuous classification of ambulation.

Musculoskeletal ultrasound (US) involves the use of highfrequency sound waves to noninvasively image underlying soft tissues and bony structures in the body. The use of dynamic US imaging of muscle contraction as a possible sensing technology for intuitive control has been recently proposed. US has the ability to provide a more detailed description of muscle contraction, without crosstalk, in real-time via detection of morphological changes in both the superficial and deep muscles with a high spatial and temporal resolution [14]. For example, changes in US image intensity are visualized during the formation of cross-bridges prior to force production [15], [16]. Multiple researchers have demonstrated the ability to classify wrist rotation and position, as well as discrete finger movements and control dexterous robotic hands with features derived from grayscale US imaging [17]–[23]. US features of the forearm muscles have also shown superior performance for the gesture recognition and muscle contraction force estimation of hand and wrist, compared to EMG [19], [24]. In two separate studies, Wang et al. and Dhawan et al. have recently demonstrated the feasibility of using US sensing for hand motion intention recognition and the control of robotic hands on amputee subjects [25], [26]. Furthermore, US has been used to estimate and predict non-weight bearing lower limb motion, as well as classify discrete phases (stance vs. swing) of the gait cycle [27]–[30].

It has yet to be explored whether US-derived features of lower-limb skeletal muscle can be used to continuously classify various modes of ambulation and how this sensing modality compares to EMG-based classification. Herein, the objective was to evaluate the feasibility of a method based on US image intensity features of the rectus femoris, vastus medialis and vastus intermedius muscles for continuous classification of five ambulation modes including: (1) level walk, (2) incline-walk, (3)



Fig. 1. Sensor placement on representative subject. (A) Ultrasound (US) probe holder placement with US transducer in place. (B) Anterior view of surface electromyography (EMG) sensor placement. (C) Posterior view of surface EMG sensor placement. (D) Complete sensor configuration including surface EMG, US with custom transducer holder and VICON reflective markers.

decline-walk, (4) stair ascent, and (5) stair descent in able-bodied subjects. We compare this US-based sensing method to features extracted from two separate configurations of surface EMG by implementing a widely-used machine learning classifier, namely, linear discriminant analysis (LDA). We hypothesized that US-based sensing would improve ambulation mode classification compared to surface EMG.

II. METHODS

A. Subjects and Ambulation Experiment

Ten able-bodied subjects completed five ambulation tasks at a self-selected speed including level walking, 10° incline walking, 10° decline walking, stair ascent and stair descent. Level walk, incline and decline trials were completed on a force-instrumented treadmill for one minute. Following treadmill trials, subjects were asked to complete five trials of 4-stair ascent followed by 4-stair descent with the normal step-overstep alternating pattern (i.e. reciprocal gait). The staircase was 20.3 cm high, 90.8 cm wide, and 30.5 cm deep. Transition strides including walk-to-stair and stair-to-walk during stair ascent and descent were labeled as the respective stair ambulation mode and included in analyses to increase the total number of stair strides available for classification, and increase the difficulty of the classification problem. This study was approved by the institutional review board at at The University of Texas at Dallas (protocol # IRB 18-33) on January 23, 2018. All subjects completed the institutional review board approved consent process prior to participation; data collection took place from October 2018 to June 2019.

B. Sensor Placement

Subjects were equipped with a custom-designed 3D printed US probe holder on their non-dominant limb. The US probe holder was placed approximately 50% of the distance between the anterior superior iliac spine and proximal base of the patella such that the US transducer will capture the belly of the anterior thigh muscles (Fig. 1(A)). The transducer of a handheld and wearable US device (mSonics, Lonshine Technologies Inc, Beijing, China) was placed transversely to collect real-time

images of rectus femoris, vastus medialis and vastus intermedius muscles. After confirmation of US transducer position and adjusting US beam depth to achieve a clear image from the transducer-skin interface to the deep vastus intermedius boundary, the transducer holder was secured around the thigh with Velcro straps to maintain the transducer position. Grayscale US images were acquired using a linear array transducer with a center frequency of 7.5 MHz, which was previously shown to have a comparable accuracy to MRI for quantification of the anterior thigh muscle parameters [31]; balancing the competing effects of spatial resolution with penetration depth. Therefore, US images were collected using a 128-element linear array transducer with a transmit frequency of 7.5 MHz and a dynamic range of 50 dB, ensuring a clear grayscale US image ranging from the superficial skin-transducer interface to the deep vastus intermedius boundary.

Eight channels of surface EMG signals were collected using the Shimmer toolkit (Shimmer3 EMG Unit, Shimmer, Dublin, Ireland). Self-adhesive and disposable pre-gelled electrodes were placed over the belly of each muscle with an interelectrode distance of 2 cm (H124SG - Covidien, Medtronic Inc., Dublin, Ireland). The skin was shaved and cleaned prior to electrode placement. Surface EMG was collected from the rectus femoris, vastus lateralis, biceps femoris, adductor magnus, tensor fascia latae, gastrocnemius, soleus and tibialis anterior muscles on the same limb as US (Fig. 1(B) and Fig. 1(C)). A custom software interface was developed to support a synchronized, real-time stream of US images and EMG signals with a temporal resolution of 1 ms. Anatomical data were recorded using VICON 3D motion capture system that tracked the location of reflective markers (Fig. 1(D)). Gait events including heel strike and toe off were recorded using Visual3D software.

C. Processing of Surface EMG and US Data

EMG sensor signals were analyzed in two separate configurations. One sensor configuration included only the five EMG sensors placed over the thigh muscles (above the knee) in order to simulate sensor placement on a subject with a transfemoral amputation (5-EMG sensing configuration). The second EMG configuration included all eight EMG sensors placed over both the thigh muscles as well as distal muscles below the knee to simulate sensor placement on a subject with a transtibial amputation (8-EMG sensor configuration). Raw EMG data were filtered with a 4th order Butterworth bandpass filter with a low cutoff at 20 Hz to remove motion artifact and a high cutoff at 450 Hz to remove high-frequency noise [32].

Continuous phase-dependent analysis was completed by segmenting EMG using an overlapping sliding window method [33]. Sliding analysis windows of 200 ms length with 100 ms overlap were used to extract six features from each window of each EMG signal [34], [35]. The six features included four time-domain features: mean absolute value, number of slope sign changes, number of zero crossings, waveform length; as well as the first two coefficients of a fourth-order auto-regressive model. An auto-regressive model is a prediction model that describes each sample from the EMG signal as a linear combination of the previous samples; a model with four

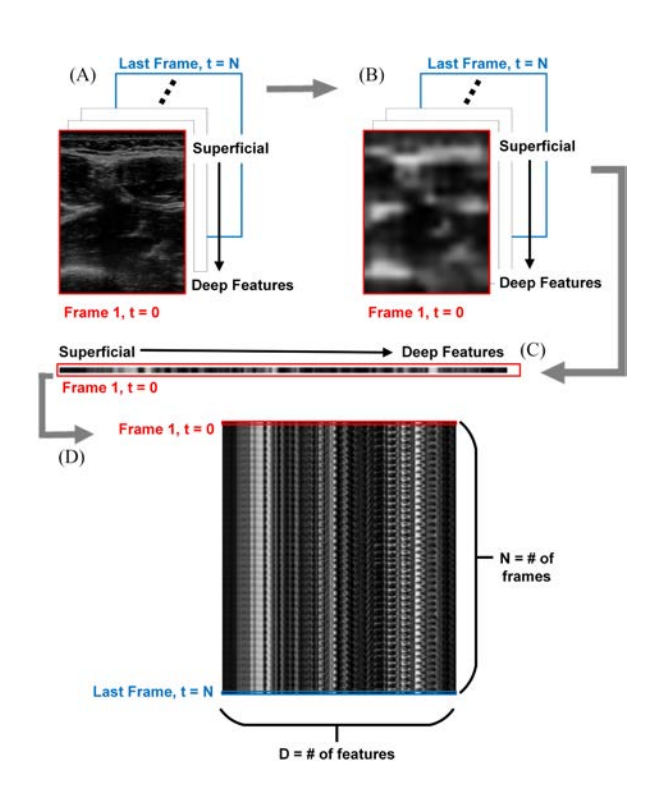


Fig. 2. Schematic Diagram of US Time Intensity Feature Methods. (A) Time series of raw B-mode US images visualizing vastus medialis (VM), rectus femoris (RF) and vastus intermedius (VI) muscles during a single walking stride. (B) Time series of 2-dimensional US features consisting of 3×3 mm blocks of mean intensity. (C) Single frame of US features transformed into 1-dimensional US intensity features ranging from superficial to deep muscle tissue. (D) Full time series of US intensity features.

orders was chosen based on previous research stating there was no improvement in discrimination accuracy for models with greater than four orders [36], [37]. This resulted in a $[N \times D]$ feature vector for each stride, where N is the number of EMG windows per stride and D is the total number of features multiplied by the number of sensors (either 6 features \times 5 or 8 sensors, depending on EMG configuration).

Grayscale US imaging can be used to visualize the hyperechoic (bright) connective tissue as well as the hypoechoic (dark) contractile tissue of muscle (Fig. 2(A)). Muscle motion is recognizable by the rapidly changing image echogenicity, or intensity, of muscle tissue. Furthermore, the frequency of change in grayscale images is related to the rate of displacement with which muscle fascicles pass through the US beam [16]. Previous researchers established a correlation between image intensity from grayscale US images with muscle contraction and muscle power [38], [39]. Additionally, fascicle behavior accessed by US has shown distinct patterns for different movements and the movement mechanics is shown to be a determinate of muscle structure and coordination, when revealed by US imaging [40]. For instance, fascicle dynamics computed using US images of the gastrocnemius medialis muscle exhibit different patterns during stair ascent and stair descent movements [41], [42]. Further, it has been demonstrated previously that US image intensity of the rectus femoris is the greatest contributor to continuous estimation of knee joint kinematics during non-weight-bearing knee flexion/extension in comparison to fascicle mechanics, muscle

thickness and aponeuroses angle [27]. Given the relevance and the low computation cost of calculating the US image intensity, we chose to create an US feature vector set consisting of multiple time-intensity features.

Mean image intensity of 3×3 mm blocks were extracted from each frame of US (Fig. 2(B)). The 3×3 mm block size was chosen to capture any changes in muscle thickness and pennation angle; previous research revealed average rectus femoris muscle thickness increases by 3.4 mm from rest to 25% of maximum voluntary contraction [43]. This 2D vector set for each frame was converted to a 1D vector set by organizing features from left to right then superficial blocks to deep blocks (Fig. 2(C)). The final US feature vector for each stride was then organized into an [N \times D] vector, where N is the number of frames per stride and D is the number of features per frame (Fig. 2(D)).

D. Ambulation Mode Classification

A linear discriminate analysis (LDA) classifier was used for continuous subject-dependent classification of ambulation mode from features of the three sensing modalities: US, 5-EMG sensors, and 8-EMG sensors. The LDA classifier was chosen for its comparable performance to more complex classifiers, as well as its potential for real-time implementation into myoelectric prostheses [34], [44]. Mean classification accuracy was reported for each sensing modality of a 5-fold within subject cross-validation randomizing the extracted feature vectors into training and testing sets, and repeating classification such that each fold was the test set once.

Confusion matrices displaying predicted ambulation mode vs. true ambulation mode are presented for each of the three sensing modalities. The confusion matrices consist of percent accuracy of classification, defined by:

$$Accuracy = \frac{\#Correctly\ Predicted\ Windows}{Total\ \#\ of\ Windows} \times 100\%$$

To account for imbalance in the amount of data in each of the five ambulation modes, precision, recall, and F1 score were calculated as additional measures to assess model performance. Precision was calculated as:

$$Precision = \frac{\#True\ Positives}{\#True\ Positives\ +\ \#False\ Positives}$$

Recall was calculated as:

$$Recall = \frac{\#True\ Positives}{\#True\ Positives\ +\ \#False\ Negatives}$$
 (3)

 F_1 score is the harmonic mean of precision and recall, and is calculated as

$$F_1 = 2 \times \frac{Precision \times Recall}{Precision + Recall} \tag{4}$$

E. Quantification of US Feature Space and Class Separability

We implemented a separability index (SI) calculation for each ambulation mode (or classes) to evaluate the contribution of information from both the superficial and deep muscle tissue available to US sensing. Previous researchers have implemented

a similar SI calculation to quantify depth information of US on hand and wrist gesture classification as well as to quantify the feature space of EMG for pattern recognition control [45], [46]. SI measures half the Mahalanobis distance from one class to its nearest class. A one-vs.-all calculation of SI was used where each individual class is compared against all the other classes and the minimum distance was chosen to represent the nearest class.

$$SI = \min_{1 \le i \le N; i \ne j} \frac{1}{2} \sqrt{(\mu_i - \mu_j)^T S_j^{-1} (\mu_i - \mu_j)}$$
 (5)

where μ_i and μ_j is the centroid of class i and class j, S_j is the covariance matrix of class j and N is the number of classes. A larger value of SI indicates more distinct classes. Each US intensity feature vector set was segmented into ten layers ranging from most superficial to deepest. The depth of each layer depended on the overall US beam depth for each subject, with the exception of the first layer, which was 6 mm for all subjects. For subjects with an overall beam depth of 50 mm, layers 2-7 were 6 mm deep and layers 8-10 were 3 mm deep. For subjects with an overall US beam depth of 70 mm layers 2-4 were 9 mm deep and layers 5-10 were 6 mm deep. There was no overlap between layers. The SI value of each layer was calculated separately for each subject then averaged to report an overall mean value for each layer.

F. Statistical Analysis

For overall classification accuracy as well as classification accuracy of each mode, a one-way repeated measure analysis of variance (ANOVA) was performed to compare the three sensing modalities. If a significant difference was detected between sensing modalities, paired *t*-tests with Bonferroni corrections were used to compare *p*-values ($\alpha = 0.05$). Additionally, to compare the SI of each US layer, a one-way ANOVA was performed. If a significant difference was detected between the US layers evaluated, *t*-tests were completed with Bonferroni corrections to compare *p*-values ($\alpha = 0.05$) between layers.

III. RESULTS

Ten able-bodied subjects (5 male, 5 female) completed five ambulation tasks including: (1) level walking, (2) 10° incline walking, (3) 10° decline walking, (4) stair ascent and (5) stair descent at a self-selected pace. Subject age ranged from 19–56 years, weight ranged from 50.7 to 82.1 kg, and height ranged from 1.50 to 1.88 m. The mean (SD) number of frames of US data of each ambulation mode are as follows, level walk: 186.8 (25.6), incline walk: 208.7 (26.7), decline walk: 184.3 (28.3), stair ascent: 36.0 (5.3), and stair descent 31.6 (3.1). Additional subject characteristics are given in Table I. All subjects reported the left leg to be their non-dominant limb.

A. Classification Accuracy of Each Sensing Modality

Five-fold cross-validation was completed for each subject to assess the average accuracy of an LDA classifier for continuous classification of five ambulation modes (level walk, incline, decline, stair ascent, and stair descent) with features from the

TABLE I DETAILED SUBJECT CHARACTERISTICS (N = 10)

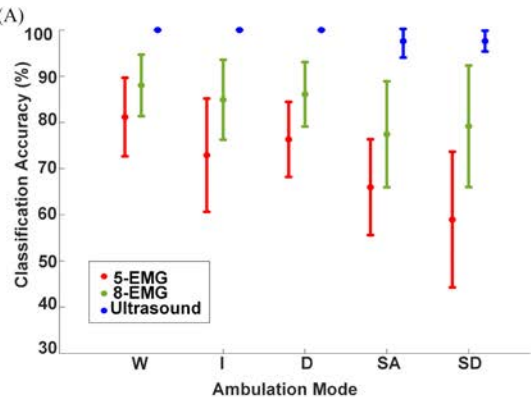
Subject Characteristic	Mean	SD
Age (years)	29.5	10.1
Mass (kg)	64.4	10.2
Height (m)	1.72	0.10
US Depth (cm)	6.0	0.5
Walk Speed (m/s)	0.80	0.14
Incline Speed (m/s)	0.64	0.10
Decline Speed (m/s)	0.62	0.10

US = ultrasound, SD = standard deviation.

three sensor sets. US sensing resulted in significantly greater mean classification accuracy across all ambulation modes of 99.8% (95% CI, 99.5 - 100%) (p < 0.001) in comparison to both the 8-EMG sensing (85.8%; 95% CI, 84.0 - 87.6%) and 5-EMG sensing (75.3%; 95% CI, 74.5 - 76.1%). F_1 score was calculated as an additional classification performance metric to account for the imbalance in the amount of data for each ambulation mode. Similar to accuracy, US sensing resulted in significantly greater F_1 score of 98.9% (95% CI, 85.2%-100%) in comparison to 8-EMG sensing (72.8%; 95% CI, 53.6%-91.9%) (p = 0.003) and 5-EMG sensing (67.1%; 95% CI, 61.9%-73.8%) (p < 0.001).

US sensing resulted in significantly greater (p < 0.001) mean classification accuracy for each ambulation mode in comparison to the 8-EMG sensor configuration (Fig. 3). The additional 3 EMG sensors placed over muscles below the knee in the 8-EMG sensor configuration significantly (p < 0.05) improved mean classification accuracy in comparison to the 5-EMG sensor configuration containing EMG sensors only over muscles above the knee for level walk, decline walk and stair ascent ambulation modes only.

Confusion matrices displaying mean percent accuracy, precision and recall are presented in Fig. 3. For US-based sensing, the only classification errors occurred during stair ascent and stair descent where stair ascent was most commonly misclassified as stair descent and vice versa. Furthermore, US-based classification produced the greatest precision (i.e., the ability of a classification model to correctly identify only the relevant data points) and recall (i.e., the ability to identify all relevant data points in a dataset) for all ambulation modes in comparison to EMG sensing. For level, incline and decline walking, there was 100% precision and recall, meaning there were no false positives or false negatives. The 5 and 8-EMG sensor configurations revealed similar trends to each other, with an overall reduction in the number of errors in the 8-EMG sensor confusion matrix compared to 5-EMG sensing. Level walk was most commonly misclassified as either incline or decline, while both incline and decline were most commonly misclassified as level walk. Both EMG-based classification models exhibited the greatest recall for level walking, while classification of incline walking exhibited the greatest precision. Similar to the US-based model, in terms of classification accuracy, precision and recall, the classification performance worsened during stair ambulation. For the 5-EMG sensor configuration, stair ascent was commonly misclassified as stair descent. However, for the 8-EMG sensor



Ultrasound		Predicted Class					
		W	- 1	D	SA	SD	Recall
	w	100.0%	0.0%	0.0%	0.0%	0.0%	100.0%
		(0.0)	(0.0)	(0.0)	(0.0)	(0.0)	(0.0)
	n I	0.0%	100.0%	0.0%	0.0%	0.0%	100.0%
Class		(0.0)	(0.0)	(0.0)	(0.0)	(0.0)	(0.0)
흥	D	0.0%	0.0%	100.0%	0.0%	0.0%	100.0%
9		(0.0)	(0%)	(0.0)	(0%)	(0%)	(0.0)
True	SA	0.0%	0.0%	0.0%	97.6%	2.4%	97.4%
0	SA	(0.0)	(0.0)	(0.0)	(3.6)	(3.6)	(4.8)
	SD	0.0%	0.0%	0.0%	2.4%	97.6%	96.8%
		(0.0)	(0.0)	(0.0)	(2.3)	(2.3)	(5.4)
Precision		100.0%	100.0%	100.0%	97.3%	97.1%	210.20
		(0.0)	(0.0)	(0.0)	(4.6)	(5.5)	

8-EMG Sensing							
		W	- 1	D	SA	SD	Recall
	w	88.0%	4.2%	5.1%	1.3%	1.4%	89.4%
True Class		(6.7)	(4.4)	(4.9)	(2.3)	(1.9)	(6.5)
	1	7.8%	84.9%	3.1%	3.0%	1.2%	84.8%
		(5.8)	(8.7)	(2.3)	(2.4)	(1.2)	(10.6)
	D	7.4%	2.3%	86.1%	1.3%	2.9%	85.8%
		(6.1)	(1.5)	(7.0)	(2.2)	(2.9)	(6.9)
	SA	3.4%	7.3%	5.9%	77.4%	5.9%	76.4%
		(5.0)	(2.8)	(5.9)	(11.5)	(5.3)	(13.9)
	SD	2.4%	2.7%	9.5%	6.2%	79.2%	75.5%
	30	(6.0)	(2.6)	(7.5)	(6.4)	(13.1)	(12.3)
Precision		85.1%	91.4%	90.3%	70.3%	67.5%	
		(8.6)	(6.1)	(5.3)	(23.9)	(67.5)	

5-EMG Sensing							
		w	1	D	SA	SD	Recall
True Class D AS	14/	81.2%	7.1%	6.1%	3.1%	2.6%	81.6%
	VV	(8.5)	(5.2)	(6.5)	(4.0)	(3.6)	(7.0)
	1	13.0%	72.9%	6.9%	4.3%	2.8%	74.1%
		(9.3)	(12.3)	(6.9)	(3.6)	(3.2)	(13.3)
	D	7.6%	6.7%	76.3%	1.6%	7.7%	75.6%
		(6.5)	(2.2)	(8.1)	(1.7)	(5.9)	(10.2)
	SA	5.5%	8.7%	4.8%	66.1%	14.8%	60.2%
		(4.3)	(3.4)	(6.2)	(10.8)	(9.0)	(18.6)
	SD	5.7%	7.0%	13.8%	12.0%	61.5%	63.5%
		(6.4)	(4.7)	(8.5)	(8.2)	(11.7)	(19.9)
Precision		79.4%	82.6%	82.2%	54.6%	43.3%	
		(11.6)	(9.0)	(11.0)	(24.7)	(17.5)	

Fig. 3. (A) Classification accuracy (mean and standard deviation (SD) from 10 subjects) and (B) confusion matrices from 5-fold cross validation for each sensing modality from each sensing modality, (5-EMG sensors, 8-EMG sensors and US), for each of the five ambulation modes, including: walk (W), incline (I), decline (D), stair ascent (SA) and stair descent (SD). Confusion matrices display mean (SD) accuracy, as well as mean precision and recall for each ambulation mode from 10 subjects.

configuration stair ascent was commonly misclassified as incline. For the 5-EMG and 8-EMG sensor configurations, stair descent was most commonly misclassified as either decline or stair ascent.

Fig. 4 displays the mean classification accuracy vs. percent of the gait cycle for a single stride of each ambulation mode. Consistent with the results presented in Fig. 3, US-based sensing

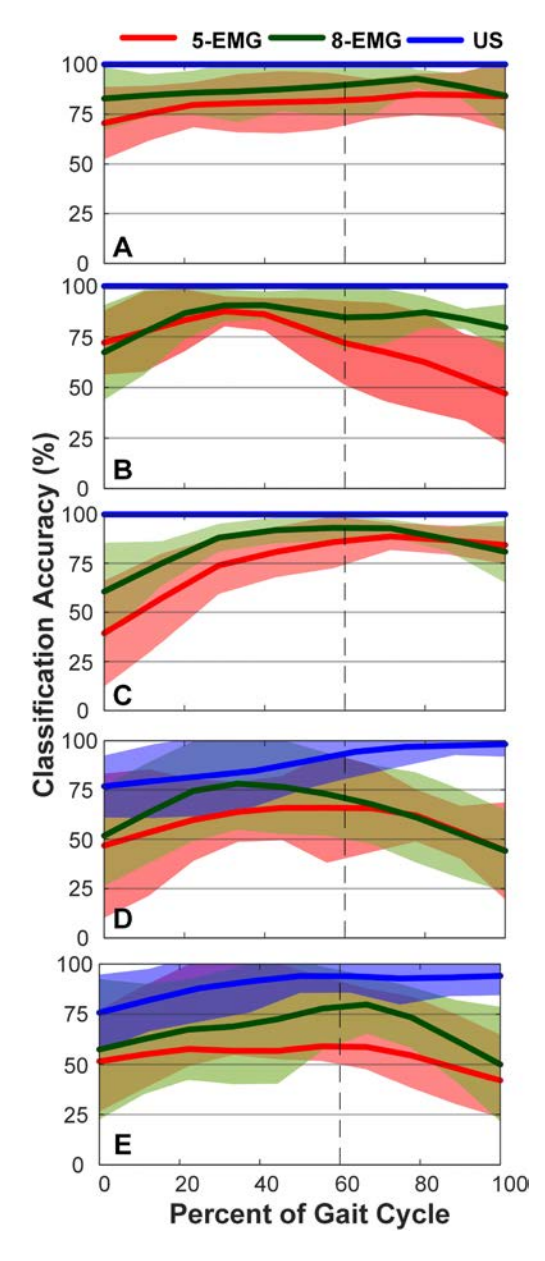


Fig. 4. Classification accuracy per stride. Mean classification accuracy per stride of all subjects using 5-EMG sensors, 8-EMG sensors and US during five locomotion modes: (A) level walking, (B) 10° incline walking, (C) 10° decline walking, (D) stair ascent, and (E) stair descent. The dashed vertical line represents the transition from stance to swing phase. Respective standard deviation shown as shaded region for all sensing modalities.

resulted in 100% accuracy during the entire gait cycle of level walk, incline and decline strides. For each of the three sensing modalities, classification accuracy remains consistent along the gait cycle for level walk strides. For both 5-EMG and 8-EMG sensing configurations, classification accuracy during incline walking decreases during swing. The opposite trend is seen for decline walking, where classification accuracy is decreased at the beginning of stance phase and increases towards toe-off and swing phase of gait. Classification accuracy during both stair ascent and stair descent with US sensing appears to increase along the gait cycle, with the greatest number of misclassifications occurring during early stance phase. In contrast to US sensing,

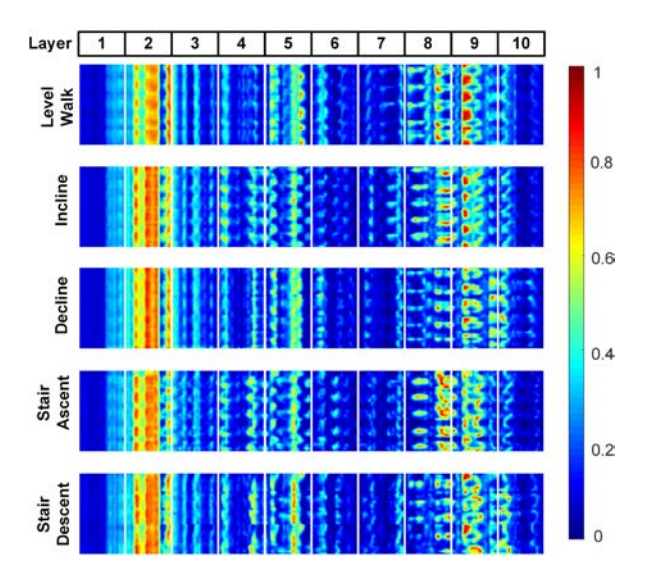


Fig. 5. Representative US Intensity Features with Layers. Color map of US intensity features from 5 strides of each ambulation mode for a single representative subject. Features have been separated into ten layers ranging from layer 1 including the most superficial US features to layer ten including the deepest US features. The range of features from 0 to 1 corresponds to magnitude of US intensity features with 0 corresponding to darkest intensity features and 1 corresponding to brightest intensity features.

classification accuracy during stair ascent for both 5-EMG and 8-EMG sensing appears to increase during stance phase to a maximum value of 80% then decrease back to the initial value of 50% during swing phase. Peak classification accuracy during stair descent for 8-EMG sensing is 80%, occurring during early swing phase, then rapidly decreases to 50% at terminal swing phase. Classification accuracy during stair descent for 5-EMG sensing is relatively stable at 50–60% during stance and decreases during swing phase.

B. Ultrasound Separability of Ambulation Mode

US image intensity features were segmented into ten layers ranging from the most superficial features in layer one to the deepest features in layer ten (Fig. 5). The first layer of US features consisted of relatively similar time-intensity values for each mode that were greater in magnitude than the subsequent layers due to the reflection of the US beam at the US transducer-skin interface. Therefore, we removed layer one from the separability index (SI) calculations in order to focus the comparison of the effect of US layers from features including only the underlying muscle tissue on the separability of each ambulation mode.

Fig. 6 shows the SI of each US layer for each ambulation mode. Higher values of SI indicate increased separability of the respective ambulation mode for that US layer. SI decreased as US depth increased with a statistically significant reduction in SI after the third layer for level walk (p=0.01), incline (p=0.001) and decline trials (p=0.005). The SI value at layer two as well as the magnitude of change between SI of superficial and deep layers of stair ambulation trials was smaller in comparison to the level walk, incline and decline trials. There was a statistically significant reduction (p=0.03) in SI after the fourth US layer for

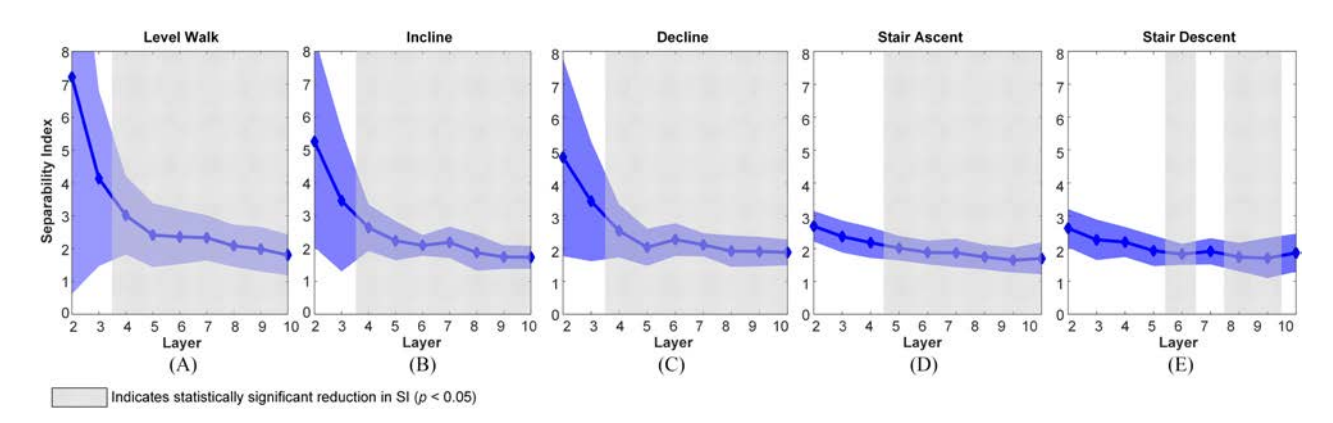


Fig. 6. Separability Index for Each Ambulation Mode. Mean of all subjects SI of nine layers of US features for each of five ambulation modes: (A) level walking, (B) 10° incline walking, (C) 10° decline walking, (D) stair ascent, and (E) stair descent. Solid blue shaded regions represent standard deviation; striped shaded regions indicate a statistically significant reduction in SI from the most superficial layer.

stair ascent trials. For stair descent trials, SI initially decreased as US depth increased, with a statistically significant reduction after the fifth layer (p=0.03), but SI increased at the seventh and tenth layers to comparable values of SI at US layers 2–4 (p>0.05).

IV. DISCUSSION

A. Comparison of US and EMG Classification Performance

This study was the first to our knowledge to evaluate the efficacy of US-based sensing relative to surface EMG for continuous classification of discrete ambulation modes in able-bodied subjects. Results from this study support our hypothesis that wearable US sensing significantly improves the classification accuracy of multiple ambulation modes in comparison to surface EMG. The evaluation of US time-intensity features with an LDA classifier resulted in 100% accuracy for level walk, incline and decline trials of all 10 able-bodied subjects. Mean classification accuracy with US-based sensing was 97.6% for both stair ascent and stair descent. In light of these results, US-based continuous classification of ambulation mode appears to be feasible and could be implemented for control of lower-limb assistive technologies. Additionally, US-based sensing may do so with less widespread sensor locations on the limb relative to other sensing modalities. Although this study evaluated able-bodied subjects, these findings may also serve to build a training database for future research involving subjects with impairments of the lower limb (e.g. adaptive learning of hand prostheses [47]).

Ideally, the control system of lower-limb assistive devices should be able to accurately detect ambulation mode and allow users to transition between various ambulation modes both effortlessly and seamlessly. Previous researchers have suggested that a continuous method for ambulation mode recognition is more efficient and informative in comparison to a phase-based method confined to discrete gait events for its ability to measure and adjust device parameters in real-time [48]–[50]. Furthermore, continuous classification could provide additional opportunities for mode switching. For instance, this style of control can be implemented in a hierarchical control structure,

where the high-level controller decides the intended activity (or ambulation mode) and a mid-level controller defines the required joint kinematic and/or kinetic trajectories, or more abstract metrics, such as joint impedance [51], mechanical energy [52] or swing clearance [53], that could be associated with different ambulation modes.

Although it is difficult to directly compare the accuracy of continuous classification of EMG signals to previous work utilizing phase-based classification, the classification accuracy of LDA with both of the EMG sensing configurations in this study was less than the classification accuracy of EMG sensing for similar ambulation modes reported by other researchers. Huang et al. [34] evaluated ambulation mode classification based on various combinations of 16 surface EMG sensors placed over muscles in the foot, shank, upper thigh and gluteal regions. When including sensors only in the gluteal and thigh regions to simulate sensor placement on a transfemoral amputee, a classification accuracy of 93% was achieved. The classification accuracy of able-bodied subjects in this study were comparable to the classification accuracy of amputee subjects with similarly placed sensors. Beyond the phase-based classification approach, one possible explanation for the difference in classification accuracy from the present study to the results described by Huang et al. is the increase in the number of surface EMG sensors, as well as a higher concentration of sensors from muscles above the knee. The present results may indicate that US sensing alone not only reduces the need for a more complex phase-based classification scheme, but also reduces the total number of sensors necessary to improve classification performance for user intent recognition.

Moreover, classification performance deteriorates due to inevitable disturbances to the sensor interface. Self-recovery or sensor fault detection has been shown to improve classification accuracy when a disturbance occurs and could be incorporated to improve the classification performance of the surface EMG signals in the present study. Furthermore, "adaptive" methods have been explored to improve EMG classification, where a change in EMG signals is detected and classification of ambulation mode reverts to mechanical sensor information then adapts the EMG pattern recognition classifier to the EMG signal changes [13]. However, it is noteworthy to mention that US sensing may suffer

from similar disturbances at the sensor (US transducer)-skin interface in regard to motion and the need for a coupling agent. Similar fault detection or adaptive techniques should be explored in the case of potential disturbances to the US transducer-skin interface.

All of the misclassification errors from US-based sensing occurred during either stair ascent or stair descent trials. This can possibly be explained by the imbalance of data for each ambulation mode, such that there were less training and testing data for stair ambulation modes in comparison to walking ambulation modes. Increasing the amount of training data for these ambulation modes to reduce the imbalance of the data set could improve classification accuracy during stair ambulation. For both stair ascent and descent ambulation modes, classification error decreased as the percent of the gait cycle increased. In other words, classification performance was worst during early stance phase through pre-toe off. It is possible this is a result of the inclusion of transition strides in the stair ascent and descent data sets. Errors during stair transition strides, as well as stair strides, could give way to troublesome clinical implications of US-based sensing within assistive devices, resulting in potentially dangerous moderate to substantial perturbations in gait [9]. Previous research investigating muscle activation patterns with surface EMG during stair ambulation indicate that the rectus femoris and vastus medialis muscles are active during only the first half of stance phase of stair ascent strides, and active during all of stance as well as terminal swing during stair descent strides [54], [55]. Therefore, the similar patterns of muscle activation during early stance could contribute to the number of misclassifications between the stair ascent and stair descent trials during this phase of the gait cycle. Inclusion of additional muscles, perhaps on the posterior thigh, could potentially increase the discrimination between these ambulation modes and improve classification accuracy.

B. Contribution of Superficial and Deep US Features

One primary question regarding the improvement in USbased classification of ambulation mode is to determine whether the improvement in performance can be attributed to the additional information from deep muscle information, or whether it is attributed to the increased dimensionality of the US signal in comparison to surface EMG. We implemented a one vs. all calculation of SI to determine the influence of depth information of US for classification of each ambulation mode. Results from the SI calculation revealed that deep muscle information does not necessarily contribute to the improved classification performance for level walk, incline and decline trials. The SI index of the second and third layers, corresponding to 12-18 mm of tissue below the first 6 mm of skin and connective tissue provided the most information to discriminate between each of these three ambulation modes. These results point to increased dimensionality or resolution of the US signal as the primary explanation, rather than the addition of information from deep muscles, for 100% classification accuracy of US-based sensing. One explanation for the decrease in SI for deeper layers could be the reduction in the energy of the sound wave as it continues

to penetrate tissue due to reflection, scattering, absorption, or dispersion [56].

In contrast, the SI value for all layers of US during stair ambulation trials decreased in magnitude in comparison to the walking trials. The SI value of stair ascent trials significantly decreased after the fourth layer (27–30 mm below the first layer). This depth could correspond to a larger area of the superficial muscles, indicating the significant contribution of information from deep fibers within the same muscle. For stair descent trials, the SI value from the second to fifth layers (24–27 mm below the first layer) and the seventh layer (6 mm at 36 mm below the first layer) provided statistically significant discriminatory information. Therefore, it is likely that the combination of an increase in resolution from superficial muscle tissue as well as the addition of information from the vastus intermedius muscle (a deep muscle in the anterior thigh) is responsible for the high classification performance of this ambulation mode. Future work should continue to evaluate the contribution of information from deep muscles available to US sensing during additional tasks, as well as the potential contribution of the US features stability over time for device implementation.

C. Potential for US Integration With Assistive Devices

Future exploration of raw US signals instead of image features may improve the potential for real-time implementation by removing the computational cost of image capturing, reconstruction and image processing steps, as well as their associated power demands. Beyond the computational and power demands, additional optimization of the size and transducer-skin interface of US imaging systems is required for this sensing modality to be incorporated into assistive devices.

Average time to process a single frame of US imaging data was 31 msec on a single CPU (Intel(R) Core i7-7700 at 3.60 GHz) computer. Currently, this is insufficient for realistic online classification. Future work aims to determine if data from the entire 128-element linear US array is needed, or rather if a subset of image intensity features from single US elements will yield similar classification accuracy. Therefore, miniaturization not only reduces the physical size of the US system, but also has potential to reduce the computational demand of the US system necessary to achieve an online control system.

Significant advances in miniaturization of US imaging systems gives way for this technology to realistically be integrated into control systems of lower limb assistive devices. Multiple researchers have explored the use of one-dimensional amplitude (A-mode) US signals for the classification of forearm muscle contraction and gesture recognition [19], [21], [57]. Furthermore, Akhlaghi *et al.* [58] concluded that there is no effect on classification accuracy when the number of US elements is reduced from 128 elements to four equidistantly spaced US elements. While the experimental set-up used in the present study may not directly translate to A-mode US-based control, these results inspire future work evaluating the use of A-mode US for the classification of ambulation as well as a reduction in the number of elements. Additionally, researchers have recently described multiple designs to reduce the size of US transducers; emerging

technology utilizes a polymer-based wearable US transducer that is low-profile and includes miniaturized sensors as flexible substrates [59], [60]. The combination of miniaturization of US imaging technology along with the improved classification performance demonstrates the potential for US imaging as a wearable sensing interface for assistive device control.

D. Limitations and Future Work

The current results demonstrate the ability of US to improve classification performance, but limitations exist that require future research. We chose to keep the classification architecture, LDA, fixed in this study to evaluate the sole effect of sensing modality. While this is a very common classifier used for applications in user intent recognition with assistive devices, optimization of the classifier architectures for these different sensing modalities remains an important area of future work. For example, neural networks have been explored for improving performance of user intent recognition based on surface EMG, mechanical sensors, as well as ultrasound-based sensors [61]–[64]. The strategies employed for US-based estimation of upper-limb motions may have the potential to translate to the lower-limb applications. For instance, using a Hidden Markov Model-based approach has shown promise to encode the temporal dependency of US features for motion prediction during transitions [65].

The imbalance in the amount of data of each ambulation mode may have negatively affected the classification performance for stair ascent and descent modes. Future data collection methods should aim to minimize the imbalance in data of all ambulation modes studied. Moreover, this study only evaluated cyclic tasks; inclusion of specific gestures as well as more complex movements, such as sit-to-stand or obstacle crossing, would reveal more information about the feasibility of US-based sensing for a truly intuitive controller for assistive devices. We aim to address these additional tasks, as well as evaluate continuous estimation of joint motion with continuous regression models as well as force-related motion protocols in future work.

Additional work is required to evaluate the stability of US features over time. Data should be collected over longer durations and multiple days to confirm that the US-based classification performance does not deteriorate over time. Additionally, the present study included able-bodied subjects only; including subjects with mobility disorders who require assistive devices and subjects with lower-limb amputations are necessary to confirm the findings of the present study. Due to the subject-dependent nature of the US features, we expect these features to change based on differences in muscle architecture of amputee subjects. However, recent research by Dhawan et al. [26] including both able-bodied subjects and subjects with an upper-extremity amputation revealed that amputee subjects were able to complete five different hand positions with >96% accuracy using the same US-based sensing as able-bodied subjects. Given the promising results of upper-extremity research involving US-based sensing, we expect that the techniques proposed in the current paper can be translated from able-bodied subjects to subjects with a lower-limb amputation with similar improvements in classification performance relative to EMG.

V. CONCLUSION

These results demonstrate the feasibility of using US imaging to reliably classify multiple ambulation modes as well as validate this classification performance versus surface EMG, one of the most commonly used sensing modalities for user intent recognition in assistive devices. The increased dimensionality of the US signal is primarily responsible for the improvement in classification performance, with information from deep muscles contributing to classification of stair ambulation. In combination with the continued miniaturization of US imaging systems, this approach could provide transformative improvements over traditional control strategies for lower-limb assistive devices, returning natural functionality and enhancing the quality of life of patients.

REFERENCES

- M. W. Brault, "Americans With Disabilities: 2010," Current Population Reports, 2012. [Online]. Available: https://www.census.gov/library/ publications/2012/demo/p70-131.html
- [2] K. Ziegler-Graham et al., "Estimating the prevalence of limb loss in the United States: 2005 to 2050," Arch. Phys. Med. Rehabil., vol. 89, no. 3, pp. 422–429, 2008.
- [3] Ö. Americas, "Power Knee," 2018. [Online]. Available: https://www.ossur.com/en-us/prosthetics/knees/power-knee
- [4] M. Bellmann et al., "Immediate effects of a new microprocessor-controlled prosthetic knee joint: A comparative biomechanical evaluation," Arch. Phys. Med. Rehabil., vol. 93, no. 3, pp. 541–549, 2012.
- [5] M. Windrich et al., "Active lower limb prosthetics: A systematic review of design issues and solutions," Biomed. Eng. Online, vol. 15, no. Suppl 3, 2016. [Online]. Available: https://www.ncbi.nlm.nih.gov/pubmed/28105948
- [6] C. D. Joshi, U. Lahiri, and N. V. Thakor, "Classification of gait phases from lower limb EMG: Application to exoskeleton orthosis," in *Proc. IEEE Point-of-Care Healthcare Technol. (PHT)*, 2013, pp. 228–231.
- [7] D. Farina et al., "The extraction of neural information from the surface EMG for the control of upper-limb prostheses: Emerging avenues and challenges," *IEEE Trans. Neural Syst. Rehabil. Eng.*, vol. 22, no. 4, pp. 797–809, Jul. 2014.
- [8] A. J. Young, T. A. Kuiken, and L. J. Hargrove, "Analysis of using EMG and mechanical sensors to enhance intent recognition in powered lower limb prostheses," *J. Neural Eng.*, vol. 11, no. 5, Sep. 2014, Art. no. 056021.
- [9] L. J. Hargrove *et al.*, "Intuitive control of a powered prosthetic leg during ambulation: A randomized clinical trial," *JAMA*, vol. 313, no. 22, pp. 2244–2252, 2015.
- [10] D. Farina et al., "Surface EMG crosstalk between knee extensor muscles: Experimental and model results," Muscle Nerve, vol. 26, no. 5, pp. 681–695, 2002.
- [11] R. H. Chowdhury et al., "Surface electromyography signal processing and classification techniques," Sensors (Basel), vol. 13, no. 9, pp. 12 431– 12 466, 2013.
- [12] M. Liu, F. Zhang, and H. H. Huang, "An adaptive classification strategy for reliable locomotion mode recognition," *Sensors*, vol. 17, no. 9, pp. 1–18, 2017.
- [13] J. A. Spanias *et al.*, "Online adaptive neural control of a robotic lower limb prosthesis," *J. Neural Eng.*, vol. 15, 1, 2018, Art. no. 16015.
- [14] T. Fukunaga et al., "Muscle architecture and function in humans," J. Biomech., vol. 30, no. 5, pp. 457–463, 1997.
- [15] R. G. Lopata et al., "Dynamic imaging of skeletal muscle contraction in three orthogonal directions," J. Appl. Physiol. (1985), vol. 109, no. 3, pp. 906–915, 2010.
- [16] A. V. Dieterich et al., "Spatial variation and inconsistency between estimates of onset of muscle activation from EMG and ultrasound," Sci. Rep., vol. 7, 2017, Art. no. 42011.
- [17] X. Yang, J. Yan, Y. Fang, D. Zhou, and H. Liu, "Simultaneous prediction of wrist/hand motion via wearable ultrasound sensing," *IEEE Trans. Neural Syst. Rehabil. Eng.*, vol. 28, no. 4, pp. 970–977, Apr. 2020.
- [18] N. Akhlaghi et al., "Real-time classification of hand motions using ultrasound imaging of forearm muscles," *IEEE Trans. Biomed. Eng.*, vol. 63, no. 8, pp. 1687–1698, Aug. 2016.

- [19] J. He et al., "Wrist and finger gesture recognition with single-element ultrasound signals: A comparison with single-channel surface electromyogram," *IEEE Trans. Biomed. Eng.*, vol. 66, no. 5, pp. 1277–1284, May 2019.
- [20] L. A. Hallock, A. Kato, and R. Bajesy, "Empirical quantification and modeling of muscle deformation: Toward ultrasound-driven assistive device control," in *Proc. IEEE Int. Conf. Robot. Autom.*, 2018, pp. 1825–1832.
- [21] J. McIntosh et al., "EchoFlex: Hand gesture recognition using ultrasound imaging," in Proc. Conf. Human Factors Comput. Syst., pp. 1923–1934, May 2017.
- [22] J. Shi et al., "Recognition of finger flexion motion from ultrasound image: A feasibility study," *Ultrasound Med. Biol.*, vol. 38, no. 10, pp. 1695–1704, Oct. 2012.
- [23] S. Sikdar et al., "Novel method for predicting dexterous individual finger movements by imaging muscle activity using a wearable ultrasonic system," *IEEE Trans. Neural Syst. Rehabil. Eng.*, vol. 22, no. 1, pp. 69–76, Jan. 2014.
- [24] X. Yang, J. Yan, and H. Liu, "Comparative analysis of wearable a-mode ultrasound and SEMG for muscle-computer interface," *IEEE Trans. Biomed. Eng.*, vol. 67, no. 9, pp. 2434–2442, Sep. 2019.
- [25] Z. Wang et al., "Ultrasonography and electromyography based hand motion intention recognition for a trans-radial amputee: A case study," Med. Eng. Phys., vol. 75, pp. 45–48, Jan. 2020.
- [26] A. S. Dhawan et al., "Proprioceptive sonomyographic control: A novel method for intuitive and proportional control of multiple degrees-offreedom for individuals with upper extremity limb loss," Scientific Rep., vol. 9, 1, 2019, Art. no. 9499.
- [27] M. H. Jahanandish, N. P. Fey, and K. Hoyt, "Lower-limb motion estimation using ultrasound imaging: A framework for assistive device control," *IEEE J. Biomed. Health Inform.*, vol. 23, no. 6, pp. 2505–2514, Nov. 2019.
- [28] M. H. Jahanandish, N. P. Fey, and K. Hoyt, "prediction of distal lower-limb motion using ultrasound-derived features of proximal skeletal muscle," in *Proc. IEEE Int. Conf. Rehabil. Robot.*, 2019, vol. 2019, pp. 71–76.
- [29] M. H. Jahanandish et al., "Gait phase identification during level, incline and decline ambulation tasks using portable sonomyographic sensing," in Proc. IEEE Int. Conf. Rehabil. Robot., 2019, vol. 2019, pp. 988–993.
- [30] Q. Zhang, K. Kim, and N. Sharma, "Prediction of ankle dorsiflexion moment by combined ultrasound sonography and electromyography," *IEEE Trans. Neural Syst. Rehabil. Eng.*, vol. 28, no. 1, pp. 318–327, Jan. 2020.
- [31] N. D. Reeves, C. N. Maganaris, and M. V. Narici, "Ultrasonographic assessment of human skeletal muscle size," Eur. J. Appl. Physiol., vol. 91, pp. 116–118, 2004.
- [32] C. J. De Luca *et al.*, "Filtering the surface EMG signal: Movement artifact and baseline noise contamination," *J. Biomechanics*, vol. 43, no. 8, pp. 1573–1579, 2010.
- [33] L. J. Hargrove et al., "Principal components analysis preprocessing for improved classification accuracies in pattern-recognition-based myoelectric control," *IEEE Trans. Biomed. Eng.*, vol. 56, 5, pp. 1407–1414, May 2009. [Online]. Available: https://www.ncbi.nlm.nih.gov/pubmed/19473932
- [34] H. Huang, T. A. Kuiken, and R. D. Lipschutz, "A strategy for identifying locomotion modes using surface electromyography," *IEEE Trans. Biomed. Eng.*, vol. 56, no. 1, pp. 65–73, Jan. 2009.
- [35] B. Hudgins, P. Parker, and R. N. Scott, "A new strategy for multifunction myoelectric control," *IEEE Trans. Biomed. Eng.*, vol. 40, no. 1, pp. 82–94, Jan. 1993.
- [36] D. Graupe, J. Salahi, and K. H. Kohn, "Multifunctional prosthesis and orthosis control via microcomputer identification of temporal pattern differences in single-site myoelectric signals," *J. Biomed. Eng.*, vol. 4, no. 1, pp. 17–22, 1982.
- [37] H. Han-Pang et al., "EMG classification for prehensile postures using cascaded architecture of neural networks with self-organizing maps," in Proc. IEEE Int. Conf. Robot. Autom. (Cat. No.03CH37422), 2003, vol. 1, pp. 1497–1502.
- [38] E. L. Cadore et al., "Echo intensity is associated with skeletal muscle power and cardiovascular performance in elderly men," Exp. Gerontol, vol. 47, no. 6, pp. 473–478, 2012.
- [39] P. W. Hodges et al., "Measurement of muscle contraction with ultrasound imaging," Muscle Nerve, vol. 27, no. 6, pp. 682–692, 2003.
- [40] J. M. Wakeling et al., "Movement mechanics as a determinate of muscle structure, recruitment and coordination," *Philosophy Trans. Roy. Soc. B: Biol. Sci.*, vol. 366, no. 1570, pp. 1554–1564, 2011.
- [41] M. Spanjaard et al., "Influence of step-height and body mass on gastrocnemius muscle fascicle behavior during stair ascent," J. Biomechanics, vol. 41, no. 5, pp. 937–944, 2008.
- [42] M. Spanjaard et al., "Lower-limb biomechanics during stair descent: Influence of step-height and body mass," J. Exp. Biol., pp. 1368–1375, 2008.

- [43] B. Chauhan, M. A. Hamzeh, and A. I. Cuesta-Vargas, "Prediction of muscular architecture of the rectus femoris and vastus lateralis from EMG during isometric contractions in soccer players," *Springerplus*, vol. 2, pp. 1–8, 2013. [Online]. Available: https://www.ncbi.nlm.nih.gov/ pubmed/24171156
- [44] K. Englehart and B. Hudgins, "A robust, real-time control scheme for multifunction myoelectric control," *IEEE Trans. Biomed. Eng.*, vol. 50, no. 7, pp. 848–854, Jul. 2003.
- [45] N. E. Bunderson and T. A. Kuiken, "Quantification of feature space changes with experience during electromyogram pattern recognition control," *IEEE Trans. Neural Syst. Rehabil. Eng.*, vol. 20, no. 3, pp. 239–246, May 2012.
- [46] J. He et al., "Wrist and finger gesture recognition with single-element ultrasound signals: A comparison with single-channel surface electromyogram," *IEEE Trans. Biomed. Eng.*, vol. 66, no. 5, pp. 1277–1284, May 2019.
- [47] T. Tommasi et al., "Improving control of dexterous hand prostheses using adaptive learning," *IEEE Trans. Robot.*, vol. 29, no. 1, pp. 207–219, Feb. 2013.
- [48] H. Huang et al., "Continuous locomotion-mode identification for prosthetic legs based on neuromuscular - Mechanical fusion," IEEE Trans. Biomed. Eng., vol. 58, no. 10, pp. 2867–2875, Oct. 2011.
- [49] D. Xu et al., "Real-time on-board recognition of continuous locomotion modes for amputees with robotic transtibial prostheses," *IEEE Trans. Neural Syst. Rehabil. Eng.*, vol. 26, no. 10, pp. 2015–2025, Oct. 2018.
- [50] H. A. Varol, F. Sup, and M. Goldfarb, "Multiclass real-time intent recognition of a powered lower limb prosthesis," *IEEE Trans. Biomed. Eng.*, vol. 57, no. 3, pp. 542–551, Mar. 2010.
- [51] N. Hogan, "Impedance control: An approach to manipulation: Part Itheory," J. Dyn. Syst., Meas. Control, Trans. ASME, vol. 107, no. 1, pp. 1–7, 1985.
- [52] T. Lenzi, L. Hargrove, and J. Sensinger, "Speed-adaptation mechanism: Robotic prostheses can actively regulate joint torque," *IEEE Robot. Autom. Mag.*, vol. 21, no. 4, pp. 94–107, Dec. 2014.
- [53] J. Mendez, S. Hood, A. Gunnel, and T. Lenzi, "Powered knee and ankle prosthesis with indirect volitional swing control enables levelground walking and crossing over obstacles," *Sci. Robot.*, vol. 5, no. 44, 2020.
- [54] Benedetti MG et al., "Muscle activation patterns during level walking and stair ambulation," in Appl. EMG Clin. Sports Med.. IntechOpen, 2012, pp. 117–130. [Online]. Available: https://cdn.intechopen.com/pdfs-wm/ 25822.pdf
- [55] M. Hall, C. A. Stevermer, and J. C. Gillette, "Muscle activity amplitudes and co-contraction during stair ambulation following anterior cruciate ligament reconstruction," *J. Electromyogr. Kinesiol*, vol. 25, no. 2, pp. 298–304, 2015.
- [56] P. N. T. Wells, "Absorption and dispersion of ultrasound in biological tissue," *Ultrasound Med. Biol.*, vol. 1, no. 4, pp. 369–376, 1975.
- [57] N. Hettiarachchi, Z. Ju, and H. Liu, "A new wearable ultrasound muscle activity sensing system for dexterous prosthetic control," in *Proc. IEEE Int. Conf. Syst., Man, Cybern.*, 2015, pp. 1415–1420.
- [58] N. Akhlaghi et al., "Sparsity analysis of a sonomyographic muscle-computer interface," IEEE Trans. Biomed. Eng., vol. 67, 3, pp. 688–696, Mar. 2020.
- [59] C. D. Gerardo, E. Cretu, and R. Rohling, "Fabrication and testing of polymer-based capacitive micromachined ultrasound transducers for medical imaging," *Microsyst. Nanoeng.*, vol. 4, pp. 1–12, 2018, Art. no. 19.
- [60] I. Almohimeed and Y. Ono, "Ultrasound measurement of skeletal muscle contractile parameters using flexible and wearable single-element ultrasonic sensor," Sensors, vol. 20, no. 13, 2020, Art. no. 3616.
- [61] A. J. Young, T. A. Kuiken, and L. J. Hargrove, "Analysis of using EMG and mechanical sensors to enhance intent recognition in powered lower limb prostheses," *J. Neural Eng.*, vol. 11, 5, 2014, Art. no. 56021.
- [62] H. Mohammadi et al., "User intent recognition for transfemoral amputees with prosthetic legs using evolutionary algorithms," in Proc. ASME Dyn. Syst. Control Conf., 2019.
- [63] Y. Li et al., "Prediction of knee joint moment by surface electromyography of the antagonistic and agonistic muscle pairs," *IEEE Access*, vol. 7, pp. 82320–82328, 2019, pp. 20–22.
- [64] L. Brausch, H. Hewener, and P. Lukowicz, "Towards a wearable low-cost ultrasound device for classification of muscle activity and muscle fatigue," in *Proc. 23rd Int. Symp. Wearable Comput.*, 2019.
- [65] A. S. Dhawan et al., "An intuitive muscle-computer interface using ultrasound sensing and Markovian state transitions," in Proc. 15th Int. Symp. Biomed. Imag., 2018, pp. 1191–1194.